Available online at www.sciencedirect.com
SCIENCE DIRECT®
Journal of Catalysis 222 (2004) 520–531
JOURNAL OF CATALYSIS
www.elsevier.com/locate/jcat

Formation of filamentous carbons over supported Fe catalysts through methane decomposition

Sakae Takenaka, Michio Serizawa, and Kiyoshi Otsuka *

Department of Applied Chemistry, Graduate School of Science and Engineering, Tokyo Institute of Technology, Ookayama, Meguro-ku, Tokyo 152-8552, Japan

Received 24 July 2003; revised 20 October 2003; accepted 6 November 2003

Abstract

Methane decomposition into hydrogen and filamentous carbons was carried out over Fe_2O_3/Al_2O_3 and Fe_2O_3/SiO_2 (7–77 wt% as Fe_2O_3) at 1073 K. The carbon yield in the methane decomposition for Fe_2O_3/Al_2O_3 (22.5 g-C/g-Fe) was greater than that for Fe_2O_3/SiO_2 (7.5 g-C/g-Fe). The difference of the catalytic performance between the two catalysts can be explained by the particle size of the catalytically active species (α-Fe metal and Fe_3C); i.e., an average particle size of catalytically active species in Fe_2O_3/Al_2O_3 did not change appreciably despite an increase of loadings, while the size in Fe_2O_3/SiO_2 became larger with loadings. Fe_2O_3 crystallites of diameters smaller than ca. 30 nm in the fresh catalysts were transformed into α-Fe metal and Fe_3C (cementite) immediately after contact of methane at 1073 K, while those of larger diameters were transformed into γ-Fe metal saturated with carbon atoms (austenite). The structures of carbons formed by methane decomposition were dependent on the types of catalytic support. Fe_2O_3/Al_2O_3 catalysts formed multiwalled carbon nanotubes and chain-like carbon nanotubes. On the other hand, Fe_2O_3/SiO_2 catalysts formed filamentous carbons which were composed of many spherical carbon particles without a hollow structure, in addition to chain-like carbon nanotubes.
© 2003 Elsevier Inc. All rights reserved.

Keywords: Supported Fe catalysts; Methane decomposition; Filamentous carbons; α-Fe metal; Iron carbides

1. Introduction

The synthesis of novel nanoscale materials is a major target in current material science research. Many research groups devoted their efforts to preparation, characterization, and application of nanostructure materials. One of the most fruitful and active fields in nanostructures is the preparation and characterization of nanostructure carbons such as filamentous carbons (carbon nanotubes and carbon nanofibers), because of their attractive physical and chemical properties [1–3]. Filamentous carbons are expected to be utilized, for example, as hydrogen-storage materials, nanoelectrical devices, nanowires, and nanosensors [4–6].

Catalytic decomposition of the molecules containing carbon atoms, such as CO and hydrocarbons is one of the promising methods for the preparation of filamentous carbons in large quantities, compared to arc-discharge [7,8] and laser vaporization methods [9] for carbon nanotube synthesis or the thermal decomposition of polymers such as polyacrylnitrile (PAN) for carbon nanofiber synthesis [10]. It is well-known that Fe, Co, and Ni supported on SiO_2, Al_2O_3, and MgO are effective catalysts for the synthesis of filamentous carbons through hydrocarbon decomposition [11–19]. In the current process for the synthesis of filamentous carbons such as vapor-grown carbon fibers, hydrocarbons such as benzene and acetylene diluted with hydrogen are decomposed over Fe-based catalysts at temperatures higher than 1273 K [1–3]. Although a high reaction temperature favors the formation of filamentous carbons with proper graphitization for Fe-based catalysts, the homogeneous pyrolysis of benzene and acetylene becomes excessive above a certain temperature depending on the carbon sources used. The homogeneous pyrolysis of benzene and acetylene produces amorphous carbons, which brings about a low purity of filamentous carbons [2]. In contrast, methane, which is the most abundant resource among all the hydrocarbons, is an ideal carbon source for production of highly graphitized filamentous carbons because of its kinetic stability at high temperatures. In most studies on the production of filamentous carbons from methane over Fe-based catalysts, methane diluted with hydrogen was contacted with the cat-

* Corresponding author.
E-mail address: kotsuka@o.cc.titech.ac.jp (K. Otsuka).

0021-9517/$ – see front matter © 2003 Elsevier Inc. All rights reserved.
doi:10.1016/j.jcat.2003.11.017

alysts at temperatures higher than 1273 K [21–25]. As for the methane decomposition over iron-based catalysts, it was reported that catalytically active species for the growth of filamentous carbons were iron species of the liquid state which were saturated with carbons [26,27]. The iron species saturated with carbons were transformed into a liquid state at temperatures higher than 1273 K. Hydrogen was cofeed in order to suppress the rapid deactivation of Fe-based catalysts due to the coverage of the catalytically active iron species with graphite layers. Recently, several research groups studied methane decomposition without cofeed of hydrogen at temperatures lower than 1073 K over Fe-based catalysts [28–30]. Ermakova et al. examined the effects of the addition of hard-reduced oxides such as SiO_2, Al_2O_3, TiO_2, and ZrO_2 into iron oxides on the catalytic activity for methane decomposition [28,29]. Iron oxides added with SiO_2 showed a high yield of filamentous carbons in the methane decomposition at a temperature range from 953 to 1073 K. They proposed that iron species with high fluidity were catalytically active species for the growth of filamentous carbons at temperatures lower than 1073 K. These results indicated that iron-based catalysts showed high activity for the methane decomposition at temperatures lower than 1273 K. However, a detailed study on the methane decomposition over Fe-based catalysts at temperatures lower than 1273 K, especially on the structure of iron species during the methane decomposition, has not been reported at the present stage.

In the present study, methane decomposition was carried out over Fe_2O_3/Al_2O_3 and Fe_2O_3/SiO_2 catalysts at 1073 K in order to examine the catalytic activities and the shape and structure of carbons formed by the reaction. In addition, structural changes of iron species during methane decomposition over these catalysts were investigated by XRD patterns and Fe K-edge XAFS spectra (XANES/EXAFS).

2. Experimental

Supported Fe catalysts used in this work were prepared by a conventional impregnation method. Al_2O_3 and SiO_2 were utilized as a catalytic supports. Al_2O_3 (JRC-ALO4) (specific surface area $= 177\ m^2\,g^{-1}$ and pore volume $= 0.66\ ml\,g^{-1}$) and SiO_2 (JRC-SIO8) (specific surface area $= 303\ m^2\,g^{-1}$ and pore volume $= 0.54\ ml\,g^{-1}$) were supplied from the Catalysis Society of Japan as reference catalysts. The catalytic support was impregnated with an aqueous solution of $Fe(NO_3)_3 \cdot 9H_2O$. The solvent of impregnated sample was evaporated to dryness at 363 K and the sample was further dried in air at 423 K for 5 h. The process was followed by calcination in air at 873 K for 5 h. The calcined catalysts were ground and sieved to smaller sizes than 60 mesh. These catalyst samples are denoted as $Fe_2O_3(X$ wt%$)/SiO_2$ and $Fe_2O_3(X$ wt%$)/Al_2O_3$ (X means loading of Fe_2O_3), hereafter.

Methane decomposition was performed with a conventional gas-flow system with a fixed catalyst bed. The powder catalyst was packed in a tubular reactor made from quartz (length and diameter of the reactor were 40 and 2 cm, respectively). Prior to the methane decomposition, the catalyst was heated at 1073 K in an argon stream. Methane decomposition was initiated by contact of methane with the catalyst at 1073 K. During the reaction, a part of exit gases from catalyst bed was sampled out and analyzed by GC. The formation rate of each product during the methane decomposition was estimated on the basis of the concentration of the product evaluated by GC and the total flow rate of effluent gases.

X-ray diffraction (XRD) patterns of the catalysts were recorded with a Rigaku RINT 2500V diffractometer using Cu-K_α radiation at room temperature.

SEM and TEM images of carbons deposited on the catalysts by the methane decomposition were measured with a Hitachi FE-SEM S-800 (field emission gun-scanning electron microscope) and with a JEOL JEM-2010F, respectively.

Raman spectra of carbons deposited on the catalyst by the methane decomposition were measured with a laser Raman spectrometer (JASCO NRS-2100). The spectra were taken with 514.5-nm line of an argon laser at room temperature. The incident laser power was adjusted to 2 mW at the sample. The spectra were recorded with a resolution of $4\ cm^{-1}$.

X-ray absorption spectra (XANES, X-ray absorption near-edge structure; and EXAFS, extended X-ray absorption fine structure) were measured on the beam-line BL-7C at the Photon Factory in the Institute of Materials Structure Science for High Energy Accelerator Research Organization at Tsukuba in Japan (Proposal Number 2002G255). X-ray absorption spectra of Fe_2O_3(14 wt%)$/Al_2O_3$ catalysts before and after methane decomposition were measured with a fluorescence mode with a Si(111) two-crystal monochromator at room temperature. The spectra of Fe_2O_3(77 wt%)$/Al_2O_3$ and Fe_2O_3 catalysts without a support after methane decomposition and of reference samples (Fe_2O_3 and Fe foil) were measured with a transmission mode at room temperature. Prior to the measurements, the catalyst samples were contacted with methane at 1073 K, followed by cooling to room temperature under Ar stream. Then, each catalyst was packed in a bag made from polyethylene under an argon atmosphere. The analyses of the spectra were performed as described elsewhere [31,32]. For EXAFS analysis, the oscillation was extracted from the EXAFS data by a spline-smoothing method. The oscillation was normalized by the edge height around 70–100 eV above the threshold. The Fourier transformation of the k^3-weighted EXAFS oscillation was performed over the range $k = 40$–$140\ nm^{-1}$ to obtain a radial structural function.

3. Results and discussion

3.1. Methane decomposition over supported Fe catalysts

Fig. 1 shows changes of the formation rate of hydrogen as a function of time on stream in the methane decom-

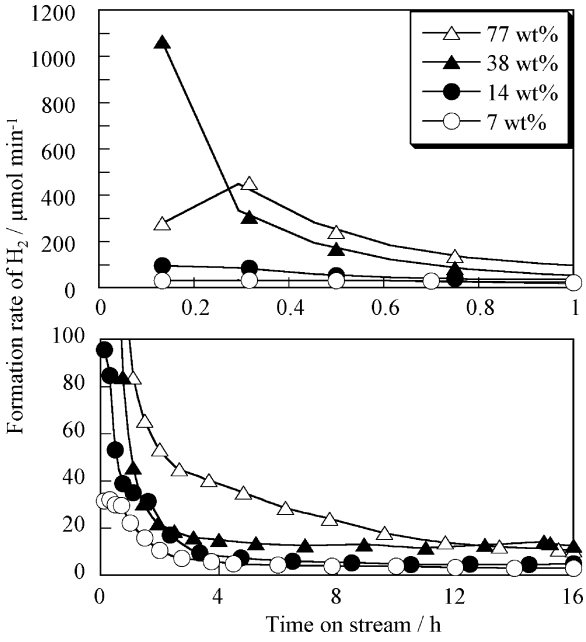

Fig. 1. Change of the formation rate of hydrogen as a function of time on stream in the methane decomposition at 1073 K over Fe_2O_3/Al_2O_3 catalysts with different loadings. Catalyst weight = 0.04 g, $P(CH_4)$ = 101.3 kPa, and flow rate of CH_4 = 70 ml min^{-1}.

position over Fe_2O_3/Al_2O_3 catalysts with different loadings at 1073 K. The upper figure indicates the results at the early stage of the reaction (< 1 h). The Fe_2O_3/Al_2O_3 catalysts decomposed methane actively at early periods of the reaction to form hydrogen. The formation rates of hydrogen at the early period became higher in the order of Fe_2O_3(7 wt%)/Al_2O_3 < Fe_2O_3(14 wt%)/Al_2O_3 < Fe_2O_3(77 wt%)/Al_2O_3 < Fe_2O_3(38 wt%)/Al_2O_3. The formation rates of hydrogen decreased quickly with time on stream for all the catalysts. Amounts of carbons deposited by the methane decomposition in 16 h were estimated by integration of the formation rates of hydrogen in Fig. 1, assuming that the stoichiometric reaction, $CH_4 \rightarrow C + 2H_2$, took place selectively. The carbon yields, C/Fe, which corresponds to moles of deposited carbons per moles of the total Fe atoms in the catalysts until 16 h of time on stream in Fig. 1, were evaluated to be 87, 75, 105, and 49 for the catalysts of 7, 14, 38, and 77 wt% loadings, respectively. The methane decomposition over these catalysts was performed at least twice in order to confirm the reproducibility of the experimental results. The carbon yields were well consistent with those evaluated from the weight of the catalysts with carbon after the methane decomposition within experimental error.

For the methane decomposition over Fe_2O_3/Al_2O_3 catalysts, attempts to observe the formation of CO, CO_2, and H_2O in addition to H_2 were made at the early period of the reaction. However, changes in the formation rates of CO, CO_2, and H_2O could not be followed under the reaction conditions, because the formation of these products stopped within 15 min after the contact of methane with the catalysts.

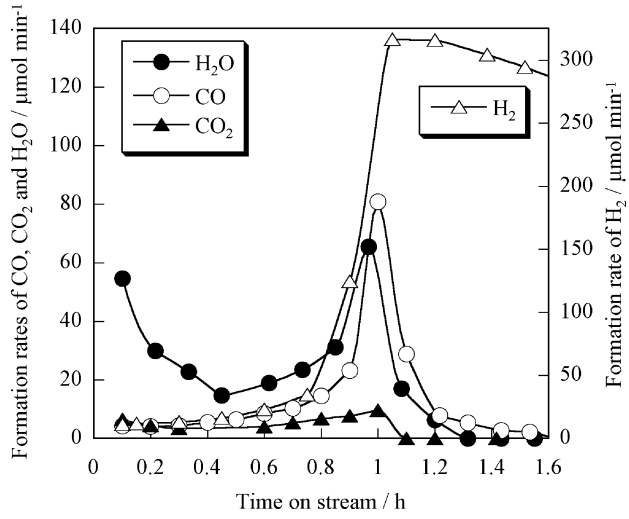

Fig. 2. Change of the formation rates of products (CO, CO_2, H_2O, and H_2) as a function of time on stream in the methane decomposition at 1073 K over Fe_2O_3(77 wt%)/Al_2O_3. Catalyst weight = 0.16 g, $P(CH_4)$ = 5.8 kPa, P(Ar) = 95.5 kPa, and flow rate = 70 ml min^{-1}.

In order to obtain kinetic curves of the formation rates of CO, CO_2, H_2O, and H_2 at the early period of the methane decomposition over Fe_2O_3/Al_2O_3 catalyst, the reaction was performed under a low partial pressure of methane (5.8 kPa) by using a large amount of the catalyst (0.16 g). The results are shown in Fig. 2. It is clear that the contact of methane with Fe_2O_3(77 wt%)/Al_2O_3 brought about the formation of H_2O, CO, CO_2, and H_2. The formation rate of H_2O decreased with time on stream (at < 0.4 h) but it increased after 0.4 h, where the formation rates of CO and CO_2 also increased. The formation rates of H_2O, CO, and CO_2 showed maxima at ca. 1 h of time on stream. These products resulted from reduction of iron oxides on Al_2O_3 with methane. The formation rate of H_2 increased sharply at > 0.8 h and reached to an apparent plateau at 1–1.6 h. The continuous formation of H_2 after 1 h could be due to the catalytic methane decomposition. These observations implied that methane decomposition was catalyzed by reduced iron species.

Fig. 3 shows XRD patterns of Fe_2O_3(77 wt%)/Al_2O_3 used for the methane decomposition at 1073 K for different times on stream. The reaction was performed under the same conditions as those shown in Fig. 2. After the methane decomposition, the catalyst samples were cooled at room temperature under Ar and exposed to air at room temperature. For the XRD pattern of the catalyst before contact with methane (a fresh catalyst), peaks due to Fe_2O_3 (hematite) were observed. These results suggested that most iron species in a fresh Fe_2O_3/Al_2O_3 were present as Fe_2O_3 crystallite. After 6 min contact with a methane stream, the peaks due to Fe_2O_3 disappeared and those due to Fe_3O_4 only could be observed. In the XRD patterns of the catalysts after 27 and 40 min of time on stream, the peaks due to Fe_3O_4 became small and the peaks due to FeO and α-Fe metal appeared at $2\theta = 36.0$, 42.0, and 60.5° and at $2\theta = 44.5$ and 65.0°, respectively. The peaks due to FeO decreased and

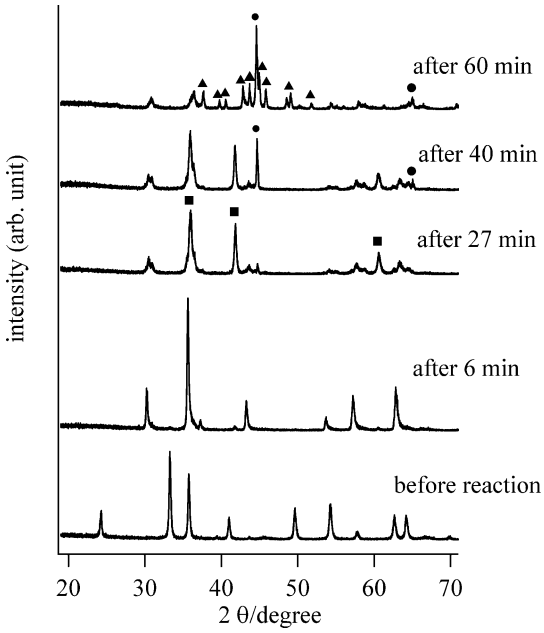

Fig. 3. XRD patterns of Fe_2O_3(77 wt%)/Al_2O_3 before and after the methane decomposition at 1073 K. FeO (■); α-Fe (●); Fe_3C (▲).

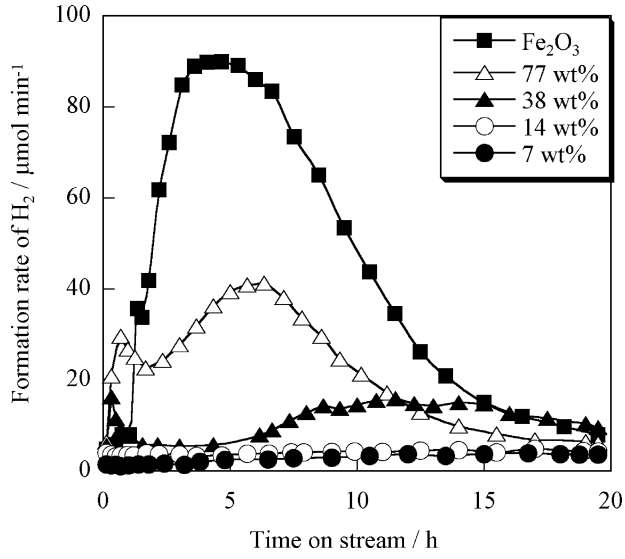

Fig. 4. Change of the formation rate of hydrogen as a function of time on stream in the methane decomposition at 1073 K over Fe_2O_3/SiO_2 catalysts of different loadings. Catalyst weight = 0.04 g, $P(CH_4) = 101$ kPa, and flow rate = 70 ml min^{-1}.

those due to α-Fe metal increased with time on stream after 27 min. In the XRD pattern of the catalyst after 60 min of time on stream, the peaks due to FeO disappeared completely and many peaks could be observed in addition to those due to α-Fe metal. These peaks could be assignable to Fe_3C (cementite) [12]. These results indicated that Fe_2O_3 in the fresh catalyst would be reduced stepwise with methane during the reaction, i.e., $Fe_2O_3 \rightarrow Fe_3O_4 \rightarrow FeO \rightarrow \alpha$-Fe metal and Fe_3C [33]. It should be noted that Fe_3C was formed at 60 min of time on stream, where the catalyst was still active for the methane decomposition as shown in Fig. 2. These results suggest that Fe_3C as well as α-Fe metal are the catalytically active species for the methane decomposition. It is likely that the decomposition of Fe_3C into α-Fe and carbons produced filamentous carbons, as proposed by several research groups [28,33].

Fig. 4 shows the formation rates of hydrogen as a function of time on stream in the methane decomposition over Fe_2O_3/SiO_2 catalysts with different Fe_2O_3 loadings at 1073 K. For all the Fe_2O_3/SiO_2 catalysts, the formation of H_2O, CO_2, and CO in addition to H_2 could be observed at the early period of the reactions, although the results for the formation of H_2O, CO_2, and CO are not shown in Fig. 4. This result indicated that iron oxides supported on SiO_2 were reduced with methane at the early period of the reaction. When the loading of Fe_2O_3 on SiO_2 increased, the formation rate of hydrogen at the early period became higher. However, the formation rates of hydrogen for Fe_2O_3/SiO_2 were significantly lower than those for Fe_2O_3/Al_2O_3. The activities of Fe_2O_3(7 and 14 wt%)/SiO_2 catalysts were especially low. The catalytic activities of Fe_2O_3/SiO_2 with 38 and 77 wt% loadings decreased until 3 h of time on stream. After 3–5 h, the formation rates of hydrogen for these catalysts showed the maxima. The carbon yields (C/Fe) at 20 h of time on stream were estimated to be < 15, 34, 35, and 33 for Fe_2O_3/SiO_2 of 7, 14, 38, and 77 wt% loadings, respectively. The C/Fe values for Fe_2O_3/SiO_2 were smaller than those for Fe_2O_3/Al_2O_3. In Fig. 4, the result for the methane decomposition over Fe_2O_3 catalyst without a catalytic support was also shown. The formation rate of hydrogen for the Fe_2O_3 catalyst also showed the maximum at ca. 5 h of time on stream. The kinetic curve of hydrogen formation for the Fe_2O_3 catalyst without a support was similar to those for Fe_2O_3(38 wt%)/SiO_2 and Fe_2O_3(77 wt%)/SiO_2. In contrast, the formation rates of hydrogen for Fe_2O_3/Al_2O_3 catalysts decreased monotonously with time on stream, irrespective of the Fe_2O_3 loadings. The feature of the kinetic curves of hydrogen formation depended on particle sizes of catalytically active iron species, as described later in detail.

3.2. Structure of iron species in the catalysts

Fig. 5 shows XRD patterns of fresh Fe_2O_3/Al_2O_3 and Fe_2O_3/SiO_2 catalysts. For XRD patterns of all the fresh catalysts except for Fe_2O_3(7 wt%)/Al_2O_3, the diffraction peaks due to Fe_2O_3 crystallite could be observed, suggesting that iron species in the fresh catalysts were present as Fe_2O_3 crystallites mainly. The XRD pattern of fresh Fe_2O_3(7 wt%)/Al_2O_3 was consistent with that of Al_2O_3 support, suggesting that iron species in fresh Fe_2O_3(7 wt%)/Al_2O_3 were highly dispersed. Average crystallite sizes of Fe_2O_3 in both fresh catalysts were estimated from full widths at half-maximum of diffraction lines due to Fe_2O_3 crystallites at $2\theta = 54.0°$ in the XRD patterns. As the loadings of Fe_2O_3 in the Fe_2O_3/SiO_2 catalysts increased from 14 to 77 wt%, average crystallite sizes of Fe_2O_3 became larger from 20 to 40 nm. In contrast, an average crystallite size

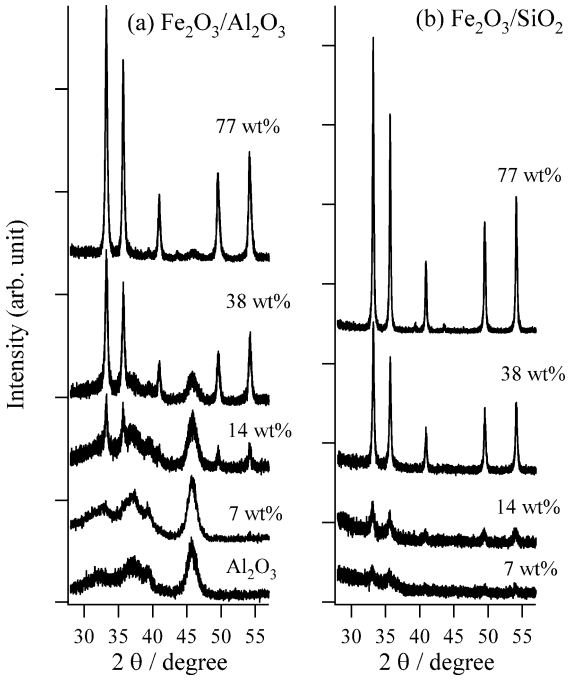

Fig. 5. XRD patterns of fresh Fe_2O_3/Al_2O_3 catalysts (a) and of fresh Fe_2O_3/SiO_2 catalysts (b).

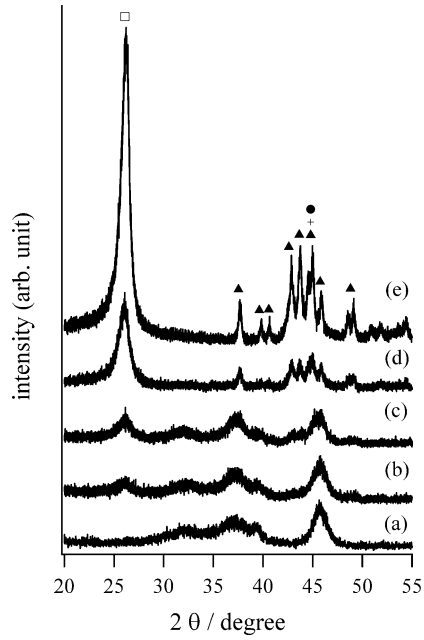

Fig. 6. XRD patterns of Fe_2O_3/Al_2O_3 catalysts deactivated for the methane decomposition at 1073 K. (a) Al_2O_3 support; (b) Fe_2O_3(7 wt%)/Al_2O_3; (c) Fe_2O_3(14 wt%)/Al_2O_3; (d) Fe_2O_3(38 wt%)/Al_2O_3; (e) Fe_2O_3 (77 wt%)/Al_2O_3. α-Fe (●); Fe_3C (▲); graphite (□).

of Fe_2O_3 in the fresh Fe_2O_3/Al_2O_3 catalysts was kept almost constant (ca. 25 nm) in the loading range from 14 to 77 wt%. As for the Fe_2O_3 sample without a support used in the reaction in Fig. 4, an average crystallite size of Fe_2O_3 was estimated to be 47 nm from the XRD results. As described earlier, the catalytic activities of Fe_2O_3/Al_2O_3 at the early period of the methane decomposition were higher than those of Fe_2O_3/SiO_2. The catalytic activities of Fe_2O_3/SiO_2 with 38 and 77 wt% loadings and of Fe_2O_3 without a support were very low at the early period of the reaction but they increased with time on stream. The catalytic performance of Fe_2O_3/Al_2O_3 and Fe_2O_3/SiO_2 would depend on a crystallite size of catalytically active iron species, which were formed during the methane decomposition by the reduction of Fe_2O_3 with methane.

Fig. 6 shows XRD patterns of Fe_2O_3/Al_2O_3 catalysts after the complete deactivation for the methane decomposition at 1073 K. The XRD patterns were measured after the methane decomposition shown in Fig. 1 (after 16 h of time on stream). In XRD patterns of all the deactivated catalysts, the peak due to graphite was observed at 2θ = ca. 26° and it became intense with loadings of Fe_2O_3. XRD patterns of deactivated Fe_2O_3/Al_2O_3 catalysts with 7 and 14 wt% loadings were quite similar to that of Al_2O_3. On the other hand, peaks due to Fe_3C could be observed for the deactivated catalysts with 38 and 77 wt% loadings and their intensities increased with the loadings. These results indicated that most of iron species in Fe_2O_3/Al_2O_3 catalysts with loadings $\geqslant$ 38 wt% were transformed into Fe_3C during the deactivation for methane decomposition at 1073 K. The structural change of iron species in Fe_2O_3/Al_2O_3 with a low loading

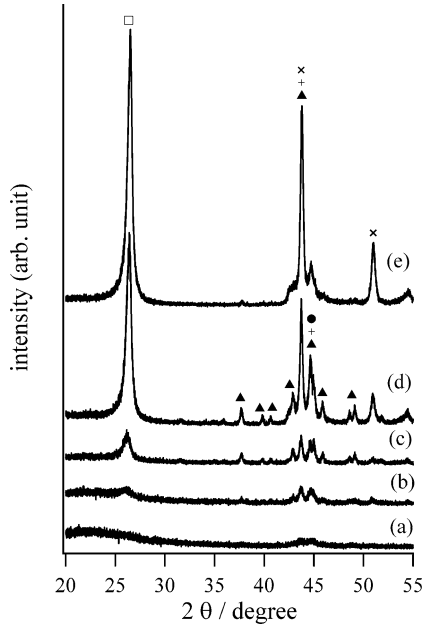

Fig. 7. XRD patterns of Fe_2O_3/SiO_2 and Fe_2O_3 catalysts deactivated for the methane decomposition at 1073 K. (a) Fe_2O_3(7 wt%)/SiO_2; (b) Fe_2O_3 (14 wt%)/SiO_2; (c) Fe_2O_3(38 wt%)/SiO_2; (d) Fe_2O_3(77 wt%)/SiO_2, (e) Fe_2O_3 catalyst. α-Fe (●); Fe_3C (▲); γ-Fe saturated with carbons (×); graphite (□).

(14 wt%) during the methane decomposition was discussed in detail later based on the results of Fe K-edge XAFS.

Fig. 7 shows XRD patterns of Fe_2O_3/SiO_2 and Fe_2O_3 without a support deactivated for the methane decomposition at 1073 K. The XRD patterns were measured after methane decomposition shown in Fig. 4 (20 h of time on stream).

In XRD patterns of all the deactivated Fe_2O_3/SiO_2 catalysts, the peaks due to Fe_3C could be observed, although the peaks for Fe_2O_3(7 wt%)/SiO_2 were very weak. In XRD patterns of deactivated Fe_2O_3(77 wt%)/SiO_2 and Fe_2O_3 without a support, new peaks could be found at $2\theta = 43.7$ and 50.5° in addition to the peaks due to Fe_3C. The XRD pattern of γ-Fe metal which is of a FCC structure shows two peaks at $2\theta = 45.8$ and 53.4°. When carbon atoms are dissolved in γ-Fe metal, the carbon atoms would expand the lattice of γ-Fe metal, which brings about the shift of the diffraction lines of γ-Fe metal to lower angles. On the basis of the XRD pattern for γ-Fe metal, the peaks at $2\theta = 43.7$ and 50.5° for deactivated Fe_2O_3(77 wt%)/SiO_2 and Fe_2O_3 without a support could be assignable to γ-Fe metal saturated with carbon atoms [34]. From the results described earlier, it is concluded that iron species in the Fe_2O_3/SiO_2 catalysts with loadings lower than 38 wt% were transformed into cementite (Fe_3C) mainly during the deactivation, while γ-Fe metal saturated with carbon atoms (austenite) in addition to cementite was formed during the deactivation of the Fe_2O_3(77 wt%)/SiO_2 and Fe_2O_3 without a support. XRD studies for Fe_2O_3/SiO_2 and Fe_2O_3/Al_2O_3 shown in Fig. 5 implied that an average crystallite size of Fe_2O_3 in fresh Fe_2O_3/SiO_2 catalysts became larger with an increase of loadings, while the size in Fe_2O_3/Al_2O_3 was kept almost constant irrespective of Fe_2O_3 loadings. It is likely that Fe_2O_3 crystallites of smaller sizes were transformed into cementite (Fe_3C) during the methane decomposition, while those of larger diameters were transformed into austenite.

Fig. 8 shows Fe K-edge XANES spectra of Fe_2O_3 (14 wt%)/Al_2O_3 samples before and after methane decomposition at 1073 K, of Fe_2O_3(77 wt%)/Al_2O_3 and Fe_2O_3 without a support deactivated for the reaction at 1073 K, and of reference samples (Fe_2O_3 and Fe foil (α-Fe metal)). Prior to the measurements of XANES and EXAFS of the catalysts, methane decomposition was performed under the same conditions as those shown in Figs. 1 and 4. Fe K-edge XANES spectra were quite different between Fe foil (spectrum a) and Fe_2O_3 (spectrum b). The threshold of XANES spectrum observed at ca. 7118–7121 eV for Fe foil was positioned at a lower energy compared to that for Fe_2O_3. In general, the threshold of XANES spectra of metal species is sensitive to the oxidation numbers of the metal. The threshold of XANES spectrum for fresh Fe_2O_3(14 wt%)/Al_2O_3 (spectrum c) was the same as that for Fe_2O_3, suggesting that iron species in the fresh catalyst were present as Fe^{3+} species which were surrounded with oxygen atoms. Contact of methane with the fresh Fe_2O_3(14 wt%)/Al_2O_3 catalyst brought about a shift of threshold in XANES spectrum to the same position as that of Fe foil as shown in Fig. 8(d). In addition, XANES spectra of the catalyst after contact with methane showed a shoulder peak at 7112 eV, which was observed in XANES spectrum of Fe foil. These results suggest that Fe^{3+} species surrounded with oxygen atoms in the fresh Fe_2O_3(14 wt%)/Al_2O_3 catalyst were reduced immediately after contact of methane at 1073 K. After deactivation of the catalyst for the methane decomposition (spectrum f), the peak at 7128 eV became unclear, while the peak could be observed clearly in spectra d and e for the catalyst which was active for the reaction. The XANES spectrum of deactivated Fe_2O_3(77 wt%)/Al_2O_3 (spectrum g) was consistent with that of deactivated Fe_2O_3(14 wt%)/Al_2O_3 (spectrum f). As described in Fig. 6, XRD patterns of the deactivated Fe_2O_3(77 wt%)/Al_2O_3 showed the formation of Fe_3C (cementite). Thus, the XANES spectra of deactivated Fe_2O_3/Al_2O_3 catalysts would be assignable to Fe_3C. These results suggest that iron species in Fe_2O_3(14 wt%)/Al_2O_3 catalysts were transformed into Fe_3C during the methane decomposition. On the other hand, the XANES spectrum of deactivated Fe_2O_3 without a support (spectrum h) was different from those of deactivated Fe_2O_3/Al_2O_3 catalysts and of two reference samples (Fe foil (α-Fe) and Fe_2O_3). XRD patterns of the deactivated Fe_2O_3 showed that iron species were present as γ-Fe saturated with carbon atoms mainly. Therefore, XANES spectrum of deactivated Fe_2O_3 may be assignable to γ-Fe saturated with carbon atoms (austenite).

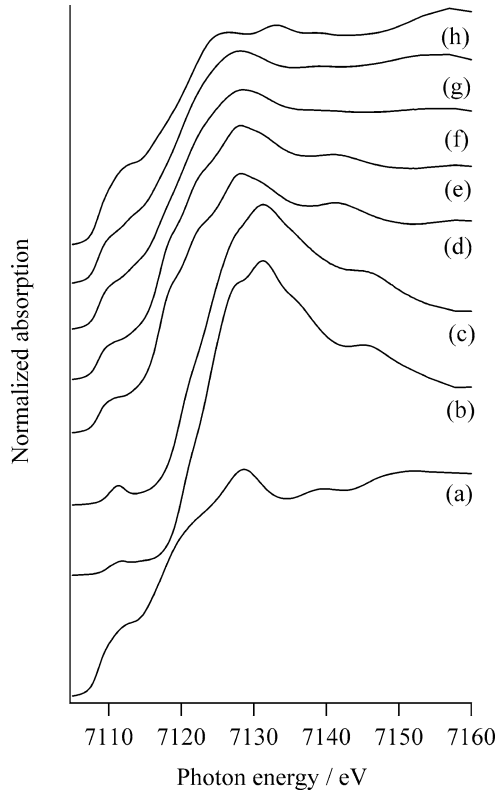

Fig. 8. Fe K-edge XANES spectra of Fe_2O_3(14 wt%)/Al_2O_3, of Fe_2O_3 (77 wt%)/Al_2O_3 and Fe_2O_3 without a support before and after the methane decomposition at 1073 K, and of reference samples (Fe_2O_3 and Fe foil). (a) Fe foil; (b) Fe_2O_3; (c) fresh Fe_2O_3(14 wt%)/Al_2O_3; (d and e) Fe_2O_3 (14 wt%)/Al_2O_3 after 5 and 20 min of time on stream of CH_4, respectively; (f and g) Fe_2O_3(14 wt%)/Al_2O_3 and Fe_2O_3(77 wt%)/Al_2O_3 after deactivation (16 h of time on stream), respectively; (h) Fe_2O_3 without a support after deactivation (20 h of time on stream).

Fig. 9 shows k^3-weighted Fe K-edge EXAFS spectra of Fe_2O_3(14 wt%)/Al_2O_3 before and after the methane decomposition at 1073 K, of Fe_2O_3(77 wt%)/Al_2O_3 and Fe_2O_3

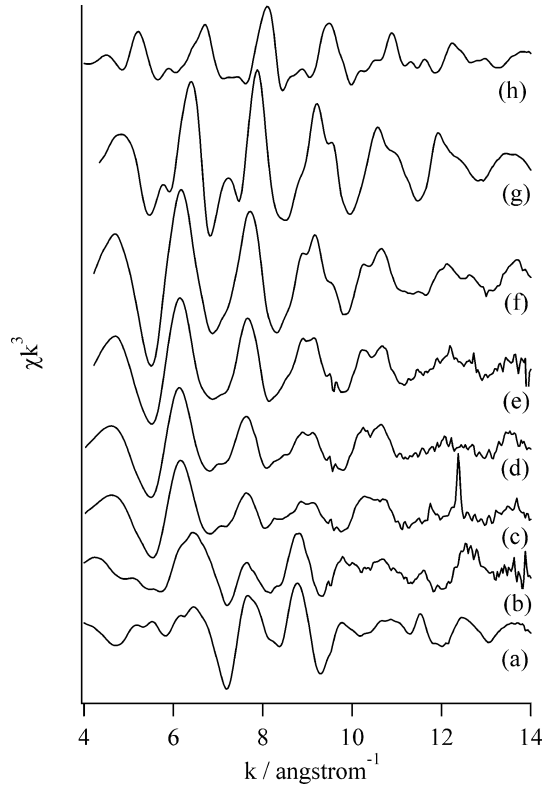

Fig. 9. k^3-weighted Fe K-edge EXAFS spectra of Fe_2O_3(14 wt%)/Al_2O_3, of Fe_2O_3(77 wt%)/Al_2O_3, and of Fe_2O_3 without a support before and after the methane decomposition at 1073 K, and of reference samples (Fe foil and Fe_2O_3). (a) Fe_2O_3; (b) fresh Fe_2O_3(14 wt%)/Al_2O_3; (c and d) Fe_2O_3(14 wt%)/Al_2O_3 after 5 and 20 min of time on stream of CH_4, respectively; (e and f) Fe_2O_3(14 wt%)/Al_2O_3 and Fe_2O_3(77 wt%)/Al_2O_3 after deactivation (16 h of time on stream), respectively; (g) Fe_2O_3 without a support after deactivation (20 h of time on stream); (h) Fe foil. Intensities of χk^3 for Fe foil and Fe_2O_3 were decreased to half.

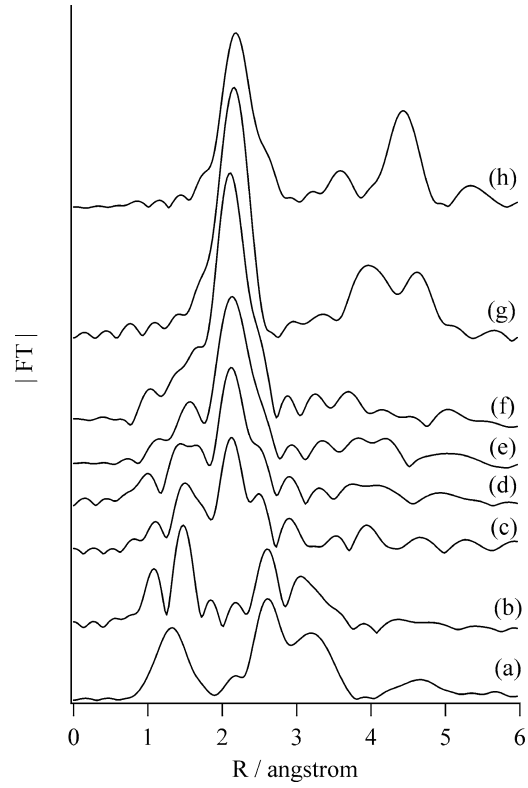

Fig. 10. Fourier transforms of k^3-weighted Fe K-edge EXAFS spectra of Fe_2O_3(14 wt%)/Al_2O_3, Fe_2O_3(77 wt%)/Al_2O_3, and Fe_2O_3 without a support before and after the methane decomposition at 1073 K, and of reference samples (Fe foil and Fe_2O_3). (a) Fe_2O_3; (b) fresh Fe_2O_3(14 wt%)/Al_2O_3; (c and d) Fe_2O_3(14 wt%)/Al_2O_3 after 5 and 20 min of time on stream of CH_4, respectively; (e and f) Fe_2O_3(14 wt%)/Al_2O_3 and Fe_2O_3 (77 wt%)/Al_2O_3 after deactivation (16 h of time on stream), respectively; (g) Fe_2O_3 without a support after deactivation (20 h of time on stream); (h) Fe foil. Intensities of |FT| for Fe foil and Fe_2O_3 were decreased to half.

without a support deactivated for the reaction, and of reference samples (Fe_2O_3 and Fe foil (α-Fe metal)). The EXAFS spectrum of a fresh Fe_2O_3(14 wt%)/Al_2O_3 catalyst (spectrum b) was similar to that of Fe_2O_3 (spectrum a), indicating that iron species in the fresh catalyst were present as Fe_2O_3. This result was consistent with the XRD pattern and XANES spectrum described earlier. Contact of methane with the fresh Fe_2O_3(14 wt%)/Al_2O_3 catalyst changed the feature of EXAFS spectrum. EXAFS spectra of Fe_2O_3(14 wt%)/Al_2O_3 catalyst after contact of methane (spectra c, d, and e) were different from those of Fe_2O_3 (a) and Fe foil (h). The patterns of EXAFS for the catalysts after the contact of methane (spectra c, d, and e) were similar to each other irrespective of the reaction time, although the amplitude of EXAFS became stronger with time on stream. In addition, the feature of EXAFS of deactivated Fe_2O_3(77 wt%)/Al_2O_3 (spectrum f) was similar to that of deactivated Fe_2O_3(14 wt%)/Al_2O_3. The EXAFS of deactivated Fe_2O_3(77 wt%)/Al_2O_3 could be assigned to Fe_3C based on the XRD studies. Therefore, it was concluded that the greater part of iron species in Fe_2O_3(14 wt%)/Al_2O_3 was transformed into Fe_3C at the early period of the reaction (5 min of time on stream), where the catalyst was active for the reaction. It is likely that catalytically active species in Fe_2O_3(14 wt%)/Al_2O_3 for the methane decomposition are Fe_3C and the decomposition of Fe_3C into α-Fe and carbon forms the filamentous carbons [28,33]. It was found that the amplitude of EXAFS for Fe_2O_3(14 wt%)/Al_2O_3 became stronger with time on stream of methane, although the pattern of EXAFS did not change with time on stream. This spectral change would be due to improvement of the crystallization degree of Fe_3C with time on stream. On the other hand, the EXAFS for deactivated Fe_2O_3 catalyst without a support (spectrum g) was different from those for deactivated Fe_2O_3/Al_2O_3 and Fe foil (α-Fe metal). The spectrum was similar to that of a metal with a face-centered cubic structure (FCC) such as Ni metal [35]. The XRD pattern of deactivated Fe_2O_3 showed the formation of γ-Fe saturated with C atoms (austenite), which has a FCC structure. Thus, iron species in Fe_2O_3 without a support were transformed into austenite during the deactivation for the methane decomposition.

Fig. 10 shows Fourier transforms (RSF, radial structural function) of k^3-weighted EXAFS spectra in Fig. 9. In RSF of a fresh Fe_2O_3(14 wt%)/Al_2O_3 (spectrum b), peaks were

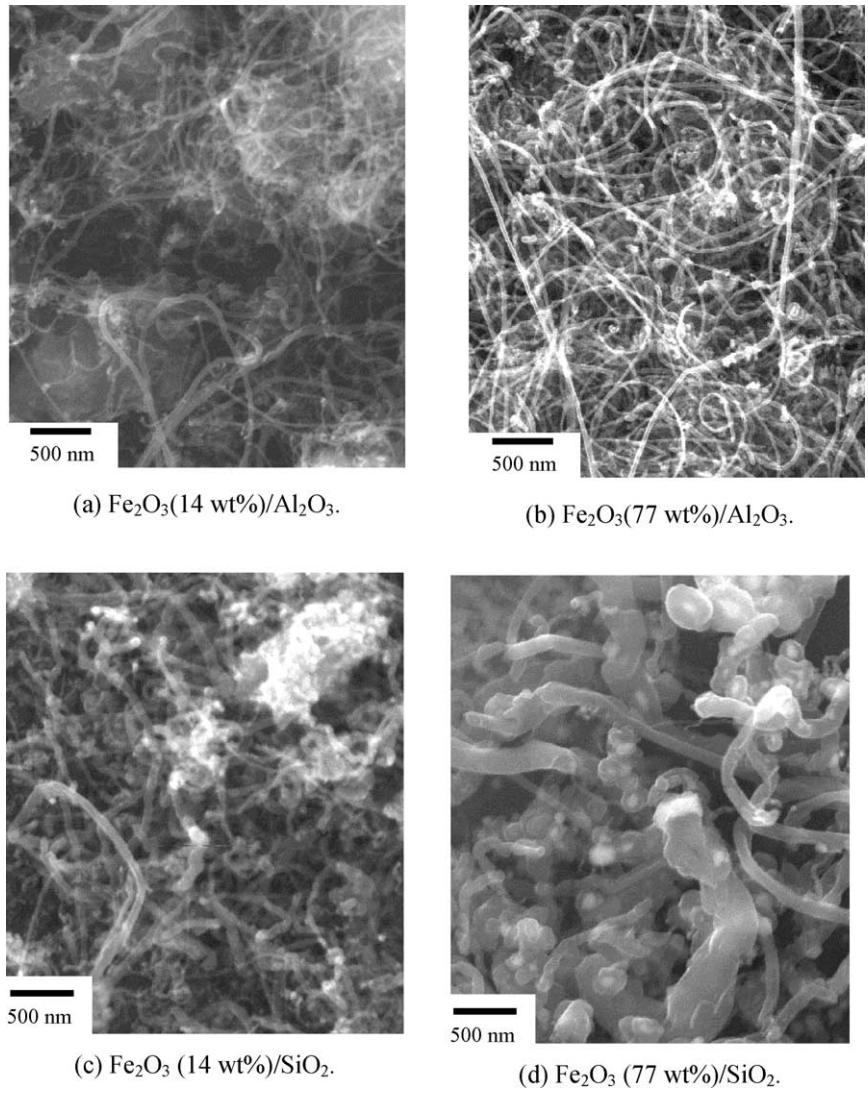

(a) Fe_2O_3(14 wt%)/Al_2O_3. (b) Fe_2O_3(77 wt%)/Al_2O_3.

(c) Fe_2O_3 (14 wt%)/SiO_2. (d) Fe_2O_3 (77 wt%)/SiO_2.

Fig. 11. SEM images of Fe_2O_3/Al_2O_3 and Fe_2O_3/SiO_2 catalysts after the deactivation for methane decomposition at 1073 K.

observed in the range of 0.9–1.7, and of 2.3–3.6 Å. The former and latter peaks could be assignable to Fe–O bonds and Fe–Fe bonds, respectively, on the basis of the spectrum of reference Fe_2O_3 (spectrum a). By contact of methane with the fresh Fe_2O_3(14 wt%)/Al_2O_3 catalyst, peaks due to Fe–O bonds became small and a new peak appeared at 2.1 Å. The peak at 2.1 Å became stronger with time on stream. Contact of methane with Fe_2O_3(14 wt%)/Al_2O_3 brought about a reduction of iron oxides. Therefore, the new peak at 2.1 Å would be due to Fe–Fe bond in reduced iron species. RSF of deactivated Fe_2O_3(14 wt%)/Al_2O_3 (spectrum e) was similar to that of deactivated Fe_2O_3(77 wt%)/Al_2O_3 (spectrum f), although the intensities of the peaks were different between the two RSFs. These RSF could be assigned to Fe_3C (cementite) on the basis of the XRD studies described earlier. On the other hand, the RSF of the deactivated Fe_2O_3 without a support (spectrum g) was different from those of deactivated Fe_2O_3/Al_2O_3 and Fe foil (α-Fe metal). The spectrum of the deactivated Fe_2O_3 was similar to that of metal with a FCC structure such as Ni metal [35], suggesting that iron species in the deactivated Fe_2O_3 without a support were transformed into γ-Fe metal saturated with carbon atoms during the methane decomposition.

3.3. Characterization of deposited carbons

Fig. 11 shows SEM images of Fe_2O_3/Al_2O_3 and Fe_2O_3/SiO_2 catalysts which were deactivated for the methane decomposition at 1073 K. The SEM images of the catalysts were measured after the reactions shown in Figs. 1 and 4. All the SEM images showed that carbons deposited on the catalysts from methane grew with a filamentous structure, as reported by many researchers [21–30]. In the SEM images of Fe_2O_3/Al_2O_3 catalysts, it was found that a diameter range of the filamentous carbons was almost the same (20–40 nm) despite different loadings. In contrast, diameters of filamentous carbons deposited on Fe_2O_3/SiO_2

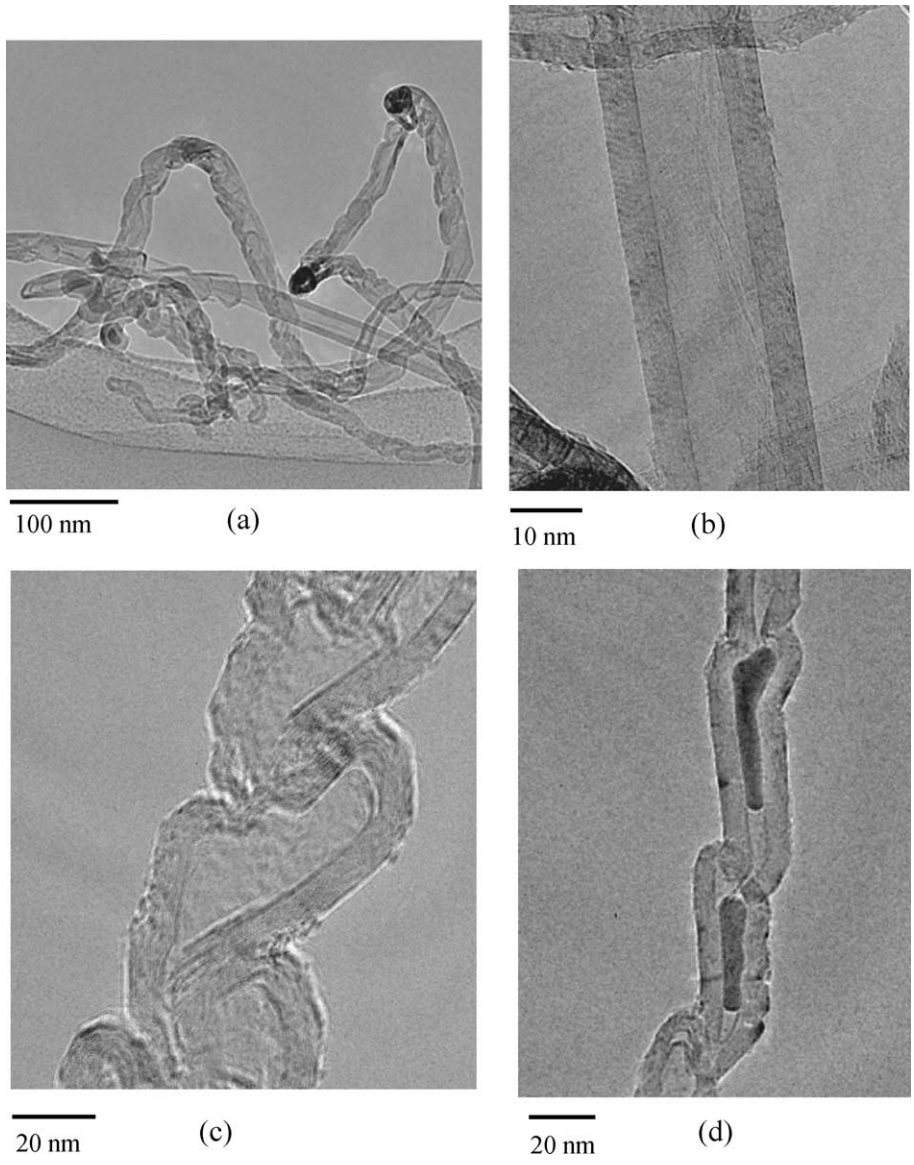

Fig. 12. TEM images of Fe_2O_3(14 wt%)/Al_2O_3 catalyst after the complete deactivation for methane decomposition at 1073 K.

catalysts became larger with an increase in loadings of Fe_2O_3. In addition, a diameter range of filamentous carbons deposited on each Fe_2O_3/SiO_2 catalyst was distributed widely, i.e., 20–80 nm for Fe_2O_3(14 wt%)/SiO_2 and 20–200 nm for Fe_2O_3(77 wt%)/SiO_2, while the diameter range for Fe_2O_3/Al_2O_3 was relatively uniform (20–40 nm). It is well accepted that metal particles such as Fe, Co, and Ni formed filamentous carbons with almost the same diameter as that of themselves by hydrocarbon decomposition [20]. These results suggested that size distributions of catalytically active species were quite different between Fe_2O_3/Al_2O_3 and Fe_2O_3/SiO_2; i.e., a particle size of catalytically active species in Fe_2O_3/SiO_2 samples was distributed widely (20–200 nm), while that for Fe_2O_3/Al_2O_3 catalyst was relatively uniform (20–40 nm).

Fig. 12 shows TEM images of carbon formed on Fe_2O_3 (14 wt%)/Al_2O_3 catalyst by methane decomposition at 1073 K. The images were measured after the reaction in Fig. 1 (16 h). As can be seen in Fig. 12a, filamentous carbons with different structures were formed by methane decomposition over the catalyst. These carbons could be classified into two types on the basis of the structures. One was multiwalled carbon nanotubes as shown in Fig. 12b. Outer and hollow diameters for multiwalled carbon nanotubes observed in TEM images ranged from 18 to 25 nm and from 10 to 15 nm, respectively. Another type was filamentous carbons with a chain-like structure, as can be observed in Fig. 12c [28,34]. The wall of a chain-like carbon fiber was of uneven structures and the hollows of this carbon fiber were divided into many cells. In addition, chain-like carbons fibers containing some cells filled with iron species could be also observed (Fig. 12d).

Fig. 13 shows TEM images of carbons deposited on a Fe_2O_3(14 wt%)/SiO_2 catalyst deactivated for methane de-

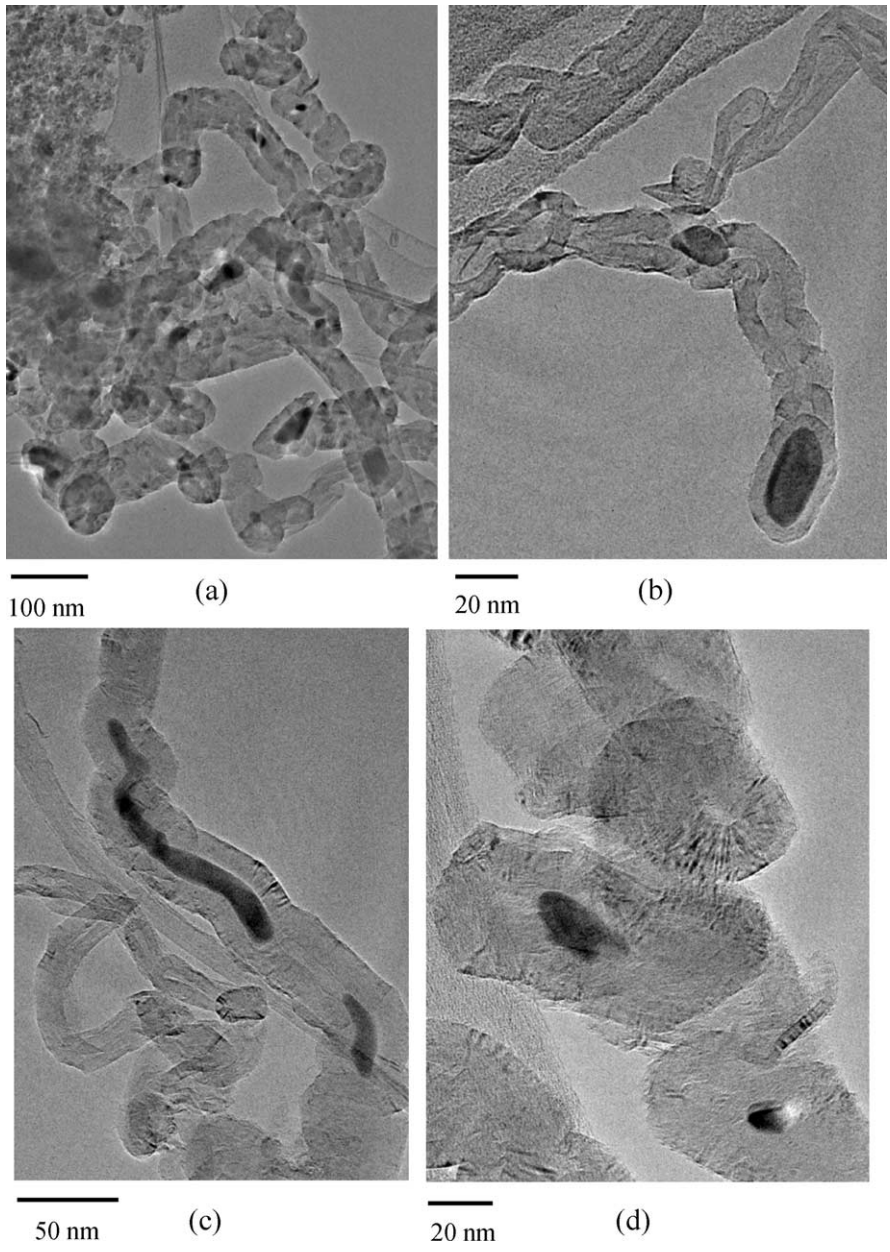

Fig. 13. TEM images of Fe_2O_3(14 wt%)/SiO_2 catalyst after the complete deactivation for methane decomposition at 1073 K.

composition at 1073 K. The images were measured after the reaction in Fig. 4 (20 h). TEM image in Fig. 13a showed that filamentous carbons with various structures were formed on the Fe_2O_3/SiO_2 catalyst. In Fig. 13b, chain-like carbon fibers could be observed and their structure was similar to that on the Fe_2O_3/Al_2O_3 shown in Figs. 12c and 12d. Concerning the chain-like carbon fibers on the Fe_2O_3/SiO_2 catalyst shown in Figs. 13b and 13c, iron species covered with carbon layers could be observed at the tip or at the center of the fibers. In addition, many filamentous carbons without a hollow structure were also observed in the images for Fe_2O_3/SiO_2 (Figs. 13a and 13d). The filamentous carbons were composed of many spherical carbon units, and iron species of sizes smaller than 20 nm were sometimes found in the units. TEM images of the spherical carbon units showed that graphite layers of the unit grew with concentric spheres from the central iron species. The filamentous carbons without a hollow structure could not be observed in the TEM images for Fe_2O_3/Al_2O_3. Baker et al. proposed that interaction of α-Fe with silica supports brings about a decrease in carbon solubility and diffusion rate of carbon atoms in the metal [36]. It is likely that this interaction of α-Fe with SiO_2 resulted in the formation of filamentous carbons different from those on Fe_2O_3/Al_2O_3 catalyst. As described earlier, the catalytic activity of Fe_2O_3/SiO_2 for the methane decomposition was significantly lower than that for Fe_2O_3/Al_2O_3. The interaction of iron species with SiO_2 would decrease the catalytic activity for the methane decomposition.

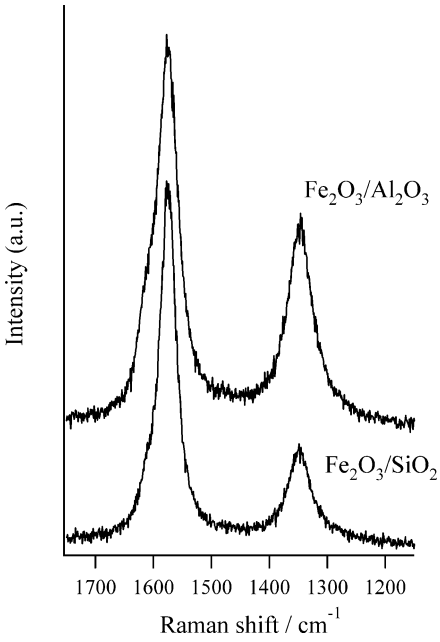

Fig. 14. Raman spectra of carbons on Fe_2O_3(14 wt%)/Al_2O_3 and Fe_2O_3 (14 wt%)/SiO_2 deactivated for methane decomposition at 1073 K.

SEM and TEM images of filamentous carbons deposited on Fe_2O_3/Al_2O_3 and Fe_2O_3/SiO_2 catalysts suggested that iron species were gradually divided into smaller ones covered with graphite layers during the methane decomposition. Based on the results of XRD and Fe K-edge XAFS studies, the iron species covered with graphite would be Fe_3C. The fragmentation of iron species, followed by coverage of them with graphite layers should deactivate the catalysts for the methane decomposition, because the iron species can not contact with methane molecules [28].

Fig. 14 shows Raman spectra of carbons deposited on Fe_2O_3(14 wt%)/Al_2O_3 and Fe_2O_3(14 wt%)/SiO_2 catalysts by the methane decomposition at 1073 K. For both Raman spectra, two bands were observed at ca. 1350 cm^{-1} (D band) and 1580 cm^{-1} (G band). The G band can be attributed to the in-plane carbon–carbon stretching vibrations of graphite layers and the D band is ascribed to structural imperfection of graphite [37,38]. In addition, a shoulder peak in the G band was found at ca. 1605 cm^{-1}. This shoulder band (denoted as D′ band) was reported to be assignable to the imperfect graphite or disordered carbons [39]. The relative intensity of G band to D band (I_G/I_D) can be regarded as an index for the crystalline order of graphite [40–42]; i.e., the graphitization degree of carbons is higher with larger I_G/I_D value. Thus, we performed the curve fitting of each Raman spectrum in Fig. 14 using three Lorentzian lines for three bands (D, D′, and G band) to estimate the value of I_D/I_G. The I_G/I_D value for Fe_2O_3/Al_2O_3 ($I_G/I_D = 1.48$) was smaller than that for Fe_2O_3/SiO_2 ($I_G/I_D = 2.50$). As described earlier, Fe_2O_3(14 wt%)/Al_2O_3 produced filamentous carbons with a hollow structure (multiwalled carbon nanotubes and chain-like carbon nanotubes) by methane decomposition, while filamentous carbons without a hollow structure in addition to chain-like carbon nanotubes were formed on Fe_2O_3(14 wt%)/SiO_2. The graphitization degree of filamentous carbons without a hollow structure would be higher compared to those with a hollow structure.

4. Conclusion

On the basis of the results described above, we concluded as follows;

1. The catalytic activity of Fe_2O_3/Al_2O_3 for the methane decomposition was higher than that of Fe_2O_3/SiO_2. The catalytic activity depended strongly on the particle sizes of catalytically active species.
2. During the methane decomposition over supported Fe-based catalysts, Fe_2O_3 particles with smaller sizes were transformed into Fe_3C (cementite), while larger ones were transformed into γ-Fe saturated with carbon atoms (austenite).
3. In the methane decomposition over Fe_2O_3/Al_2O_3 catalysts, multiwalled carbon nanotubes and chain-like carbon fibers were formed, while Fe_2O_3/SiO_2 formed carbon fibers which were composed of many spherical carbon units, in addition to chain-like carbon fibers.

References

[1] K.P. de Jong, J.W. Geus, Catal. Rev. Sci. Eng. 42 (2000) 481.
[2] L.P. Biro, C.A. Bernardo, G.G. Tibbetts, Ph. Lambin (Eds.), Carbon Filaments and Nanotubes: Common Origins, Differing Applications?, Kluwer Academic, Boston, 2000.
[3] G. Benedek, P. Milani, V.G. Ralchenko (Eds.), Nanostructured Carbon for Advanced Applications, Kluwer Academic, Boston, 2000.
[4] A.C. Dillon, K.M. Jones, T.A. Bekkedahl, C.H. Kiang, D.S. Bethune, M.J. Heben, Nature 386 (1997) 377.
[5] W.A. de Heer, A. Chatelein, D. Ugarte, Science 270 (1995) 1179.
[6] S. Fan, M.G. Chapline, N.R. Franklin, T.W. Tombler, A.M. Cassel, H. Dai, Science 283 (1999) 512.
[7] S. Iijima, Nature 354 (1991) 56.
[8] T.W. Ebbesen, P.M. Ajayan, Nature 358 (1992) 220.
[9] T. Guo, P. Nikolaev, A. Thess, D.T. Colbert, R.E. Smalley, Chem. Phys. Lett. 243 (1995) 49.
[10] D.D. Edie, Carbon 36 (1998) 345.
[11] R.T.K. Baker, M.A. Barber, P.S. Harris, F.S. Feates, R.J. Waite, J. Catal. 26 (1972) 51.
[12] A. Sacco, P. Thacker, T.N. Chang, A.T.S. Chiang, J. Catal. 85 (1984) 224.
[13] P.K. de Bokx, A.J.H.M. Kock, E. Boellaard, W. Klop, J.W. Geus, J. Catal. 96 (1985) 454.
[14] A. Govindaraj, E. Flahaut, Ch. Laurent, A. Peigney, A. Rousset, C.N.R. Rao, J. Mater. Res. 14 (1999) 2567.
[15] T.V. Choudhary, C. Sivadinarayana, C.C. Chusuei, A. Klinghoffer, D.W. Goodman, J. Catal. 199 (2001) 9.
[16] L.B. Avdeeva, O.V. Goncharova, D.I. Kochubey, V.I. Zaikovskii, L.M. Plyasova, B.N. Novgorodov, Sh.K. Shaikhutdinov, Appl. Catal. A 141 (1996) 117.
[17] M.A. Ermakova, D.Yu. Ermakov, G.G. Kuvshinov, L.M. Plyasova, J. Catal. 187 (1999) 77.

[18] P. Wang, E. Tanabe, K. Ito, J. Jia, H. Morioka, T. Shishido, K. Takehira, Appl. Catal. A 231 (2002) 35.
[19] S. Takenaka, K. Kobayashi, H. Ogihara, K. Otsuka, J. Catal. 217 (2003) 79.
[20] R.T.K. Baker, Carbon 27 (1989) 315.
[21] A. Peigney, Ch. Laurent, A. Rousset, J. Mater. Chem. 9 (1999) 1167.
[22] E. Flahaut, A. Govindaraj, A. Peigney, Ch. Laurent, A. Rousset, C.N.R. Rao, Chem. Phys. Lett. 300 (1999) 236.
[23] J.-F. Colomer, C. Stephan, S. Lefrant, G. van Tendeloo, I. Willems, Z. Konya, A. Fonseca, Ch. Laurent, J.B. Nagy, Chem. Phys. Lett. 317 (2000) 83.
[24] B.C. Liu, S.H. Tang, Z.L. Yu, B.L. Zhang, T. Chen, S.Y. Zhang, Chem. Phys. Lett. 357 (2002) 297.
[25] L. An, J. Owens, L.E. McNeil, J. Liu, J. Am. Chem. Soc. 124 (2002) 13688.
[26] F. Benissad, P. Gadelle, M. Coulon, L. Bonnetain, Carbon 26 (1988) 425.
[27] G.G. Tibbetts, M.P. Balogh, Carbon 37 (1999) 241.
[28] M.A. Ermakova, D.Y. Ermakov, A.L. Chuvilin, G.G. Kuvshinov, J. Catal. 201 (2001) 183.
[29] M.A. Ermakova, D.Y. Ermakov, Catal. Today 77 (2002) 225.
[30] L.B. Avdeeva, T.V. Reshetenko, Z.R. Ismagilov, V.A. Likholobov, Appl. Catal. A 228 (2002) 53.
[31] T. Tanaka, H. Yamashita, R. Tsuchitani, T. Funabiki, S. Yoshida, J. Chem. Soc., Faraday Trans. 184 (1988) 2987.
[32] S. Yoshida, S. Takenaka, T. Tanaka, H. Hirano, H. Hayashi, Stud. Surf. Sci. Catal. 101 (1996) 871.
[33] C. Emmenegger, J.-M. Bonard, P. Mauron, P. Sudan, A. Lepora, B. Grobety, A. Zuttel, L. Schlapbach, Carbon 41 (2003) 539.
[34] Ch. Laurent, A. Peigney, A. Rousset, J. Mater. Chem. 8 (1998) 1263.
[35] S. Takenaka, H. Ogihara, K. Otsuka, J. Catal. 208 (2002) 54.
[36] R.T.K. Baker, J.J. Chludzinski, C.R.F. Lund, Carbon 25 (1987) 295.
[37] K. Sinha, J. Menendez, Phys. Rev. B 41 (1990) 10845.
[38] R.J. Nemanich, S.A. Solin, Phys. Rev. B 20 (1979) 392.
[39] H. Darmstadt, L. Sümmchen, J.-M. Ting, U. Roland, S. Kaliaguine, C. Roy, Carbon 35 (1997) 1581.
[40] R.O. Dilion, J.A. Woollam, V. Katkanant, Phys. Rev. B 29 (1984) 3482.
[41] T. Jawhari, A. Roid, J. Casado, Carbon 33 (1995) 1561.
[42] A. Cuesta, P. Dhamelincourt, J. Laureyns, A. Martinez-Alonso, J.M.D. Tascon, Carbon 32 (1994) 1523.